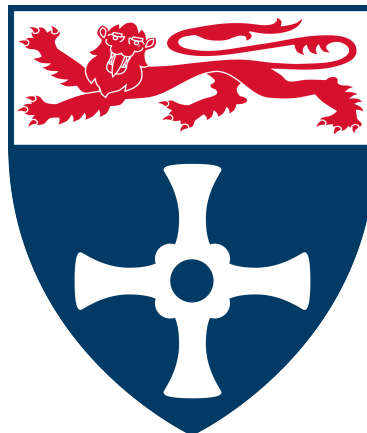


Evaluating the Feasibility of Automated Lesion Masking for Normative Lesion Network Mapping

Ewan Walker, Corey Ratcliffe, Peter Taylor

A thesis presented for the degree of
Bachelor of Science in Computer Science



Department of Computer Science
Newcastle University
England

May 7, 2025

8,732 words

Contents

1	Introduction	4
1.1	Context	4
1.2	Problem Statement	7
1.3	Aims & Hypotheses	7
1.4	Literature Review	7
2	Methodology	9
2.1	Material and Participants	9
2.2	Meningioma Image Preprocessing	9
2.3	The Normative Data Pipeline	10
2.4	The Subject Specific Pipeline	11
2.5	Statistical Analysis	12
3	Results	13
3.1	Mask Comparison	15
4	Discussion	19
4.1	Mask Comparison	19
4.2	Tractography Comparison	20
4.3	Limitations & Future Plans	22
4.4	Conclusion	22
5	Appendix	27
5.1	Structural Pipeline Code	27
5.2	Diffusion Pipeline Code	30
5.3	Meningioma Seeded Tractography Code	34

Acknowledgments

Thank you to Corey Ratcliffe for mentoring me; his advice, patience, and feedback throughout this project have been exemplary. Thanks also to Peter Taylor for allowing me to undertake this research with the CNNP lab, and to my parents for their support throughout university and for being there for me, whatever the occasion.

Meningiomas are brain tumours originating in the meninges, which account for around 40 % of all intracranial tumours. Delineating meningiomas on MRI scans is a time-consuming task that requires an experienced Neuroanatomist or otherwise qualified professional. Fortunately, many automated segmentation algorithms forego these requirements, showing great promise for use in research. However, they need to be evaluated with independent studies. The use of masks for normative lesion network mapping

We generate masks from diffusion-weighted imaging data alongside structural T1-CE MRI scans from 5 different subjects, each diagnosed with meningiomas, to compare the downstream error introduced by the automatic generation of the lesion masks. By comparing automatically generated lesion masks with masks manually delineated by an experienced professional, alongside tractograms seeded from them using methods such as the Sørensen–Dice index, we aim to evaluate the efficacy of a novel deep learning based meningioma segmentation algorithm. We applied a reproducible pipeline on research-quality data, quantitatively evaluating the performance of automated meningioma masking for use in normative lesion network mapping and provided evidence of promise shown for use in a research capacity, outlining the benefits of time reduction, cost savings and autonomy, but with a slight tradeoff of accuracy if implemented.

1 Introduction

Meningiomas are brain tumours originating in the meninges, which account for around 40 % of all intracranial tumours (Ostrom et al., 2021). A tumour is an uncontrolled growth of tissues inside the brain. To ascertain information about the tumour, it can be masked, and currently, the gold standard technique for masking tumours is manual (by hand), by an experienced professional, which is time-consuming and thus expensive. However, the lesion masks produced have many uses, such as resection (surgery) planning, where it is used to help predict post-surgical effects and risks associated with the resection. One method to predict these effects is lesion network mapping.

Tractography is a technique for estimating probable directions of white matter tracts *in vivo* by traversing a continuous path of greatest diffusivity through voxels (and tensors) until a predefined terminal condition is met from an initial set of seed points (Bammer et al., 2003). One use of tractography is lesion network mapping, which identifies the distribution of regions likely to be functionally affected by a given brain lesion (Boes et al., 2015). The effects of brain tumours can be severe, such as seizures that may occur after resection. By linking the focal effect of the tumour to distal regions of the brain, we can predict the possibility of recurrent post-operative seizures, this prediction also plays an important role in surgical planning.

Deep-learning techniques such as a convolutional neural network (CNN) or a generative adversarial network (GAN) can be used separately or in combination, and for example, analyse features defined in matched pair training and estimate where a mask would be in a novel MRI scan. This estimation could vary from the hand-delineated lesion mask based on model performance, and in that case, the automatic tractogram could vary from the manual mask.

In cases where individual patients' data is not available, Normative data, data that characterise what is usual in a defined population at a specific point or period of time (O'Connor, 1990), can be used to estimate certain biological features such as general white matter structure.

We have applied a reproducible pipeline to research-quality data to quantitatively evaluate the efficacy of automatically delineated meningioma masks using deep learning tissue classification models for normative lesion network mapping with tractography and provided evidence about the feasibility of automated masking.

1.1 Context

This study encompasses a broad range of subjects and incorporates them into different aspects of the research, such as the analysis and methodology. This section aims to introduce and provide high-level explanations of some of the core subjects, to then build off in later sections where they are utilised.

1.1.1 Clinical Sample - Structural Data

For the initial input of the structural pipeline, we have used T1-weighted (T1w) magnetic resonance imaging (MRI) scans in which fatty tissues are shown as white compared to tissues with a higher relative water concentration. The scans are also contrast-enhanced (CE), where the subject is injected with a gadolinium bolus (Contrast Dye), making certain pathologies more visible. These show us the position and size of the meningioma.

1.1.2 Normative Sample - Diffusion Imaging Data

For the diffusion pipeline, we take a subset of healthy control patients and measure the diffusion of water throughout their brains to map the anatomy of fibres that comprise the underlying structure of the brain. This movement should be random, but when constrained, it is measurably anisotropic. This data can then be averaged across the entire subset of healthy subjects to produce a normative template.

1.1.3 Intracranial Lesions

Broadly, an intracranial lesion is damage to, or an abnormality in, brain tissue with any number of potential causes, such as trauma, malformation, age related damage. In the context of this study, it will be used interchangeably with ‘brain tumour’, as we will be focusing on abnormal masses of meningioma and their downstream effects on white matter and grey matter connectivity.

1.1.4 Meningiomas

Meningiomas are mostly benign, with about 20% showing more aggressive behaviours and a higher tendency to recur.(Behling et al., 2021) However, a study conducted by Englot et al. showed that approximately 29% of patients present with preoperative seizures, which resolved postoperatively in 69.3% of patients. (Englot et al., 2016)

1.1.5 Meningioma Related Seizures

MRS (Meningioma-related Seizures) are characterised by focal onset and can present with secondary generalisation, meaning that seizures initially propagate from a single discrete region, and over time spread to include seizure activity in both hemispheres.(Fisher et al., 2017) Early evidence has implicated a mutation in the NF2 gene in being associated with preoperative seizures, but a comprehensive mechanism has yet to be defined. (Gupte et al., 2020)

1.1.6 Structural & Diffusion Imaging

Structural (Anatomical) imaging is a set of approaches used to visualise anatomical structures within the body, and is often integral in the evaluation and

treatment of medical conditions. This includes MRI and CT (Computed Tomography) scans, which can provide *in vivo* images that are sensitive to the presence of different tissues.

Diffusion Weighted Imaging (DWI) is an MRI modality that can characterise white matter fibres by tracking the restriction of water movement (diffusion) in the capillary-like fibres.(Basser et al., 1994) Information acquired through DWI can be resolved into a directional element, a 3-dimensional tensor, which establishes likely fibre orientation by comparing the anisotropy (i.e. inequality) of all the measured diffusion in a single spatial region, as unrestricted diffusion is random and therefore spherical (isotropic). From the tensor, it is possible to resolve metrics like Fractional Anisotropy, which is a scalar value equal to the amount of coherent diffusion in the principal diffusion direction of the tensor (and the estimated fibre). (Hu & Hoch, 2021)

1.1.7 White Matter & Grey Matter

Clusters of neurones (grey matter) and bundles of myelinated axons (white matter), which propagate electrochemical signals between neurons, make up the structural architecture of the brain. Together, they form one large neural network or a series of smaller interconnected neural networks. In the context of computing neural networks, grey matter can be thought of as nodes, and white matter tracts serve as edges. (Moody et al., 2021)

1.1.8 Automated Tissue Classification

The brain can be classified into the white matter, the grey matter, the cerebrospinal fluid, and several surrounding structures, the meninges (comprised of the dura mater, arachnoid layer, and pia mater). Tissue properties of different brain regions have been comprehensively described, and an expert can quickly visually identify abnormalities in an MRI, which may constitute pathology. There have been many proposed tissue classification models to automate this process, such as the Automated Meningioma Segmentation (AMS) tool from NeuroNets (Rajchl et al., 2018). These models are developed to detect and label outliers in MRI, to facilitate the quick identification of pathology.

1.2 Problem Statement

The current gold standard technique to delineate a Brain lesion is to be done manually by an experienced professional; this takes a long time and is, by that fact, expensive. Automatic delineation foregoes these drawbacks at the possible cost of accuracy, however, it is yet to be quantitatively evaluated by an independent study. Having no quantified magnitude of difference between the two methods means implementation of automatic delineation in any processes is risky. For normative lesion network mapping, knowing the accuracy of the generated mask is essential in gauging whether the lesion network seeded from it is as accurate as possible when predicting effects in distal regions shown through tractography to be downstream of white matter fibres *proxima* to the lesion.

If the efficacy of automatic lesion masking was quantified by an independent study, the element of risk when implementing it into processes is removed, and instead, a margin of error that is quantified in said study needs to be contemplated and accounted for.

1.3 Aims & Hypotheses

This study aims to evaluate the feasibility of automated lesion masking for normative lesion network mapping. We will compare the pre-surgical structural connectivity profiles of manually defined versus automatically defined meningioma-based lesion network masks using normative data. The study involves:

- Computing the overlap of manually and automatically defined meningioma masks in an exemplar subset of presurgical MRI data.
- Measuring the overlap of streamlines seeded from manually and automatically defined lesion masks.
- Quantifying the ability of automatic masks to provide a feasible alternative to manual delineation for lesion-network mapping.

We expect to find that the trade-off in accuracy of automated lesion masking is low enough to justify its use in a research capacity as a low-cost alternative to hand delineation, where there is a large set of patients who have brain tumours that require delineation for normative lesion network mapping. We also expect that tractography seeded from automatic masks is a viable method for assessing structural connectivity in brain tumours.

1.4 Literature Review

This study relies on several key references, and in this section, we provide a brief overview of the paper with its relevance to our research. We then provide evidence to support the reliability of the source.

1.4.1 Deep Neural Networks for Brain Meningioma Segmentation

Citation: Boaro et al. (2022)

Overview: Demonstrates a convolutional neural network that performs automated meningioma segmentation and volume estimation on MRI scans. It measures the performance using methods such as Dice similarity coefficient, precision, recall, and F1 score.

Relevance: This paper demonstrates the algorithm that will be implemented into the pipeline to automatically segment the meningiomas and estimate the volume. It also contains test data from when they run the software on the scans without pre-processing the MRI scan, nor does it process the image post-segmentation. This is useful for evaluating the performance of the pipeline implemented in this research.

Source Evaluation: Published in the reputable, peer-reviewed journal Scientific Reports, it has been through review and held to high standards. The authors have credible backgrounds in fields such as computer vision, machine learning, and medical imaging, and this paper has been previously cited many times.

1.4.2 The ANTsX Ecosystem for Quantitative Biological and Medical Imaging

Citation: Tustison et al. (2021)

Overview: A library containing top-performing algorithms used for processing and analysing biological and medical imaging data. Various types of tools and algorithms are included in the ANTsX ecosystem, including image registration, segmentation, and statistical analysis.

Relevance: This library contains some of the tools needed for data processing and analysing the images for this project and is an improved version of the previously established ANTs library from 2008.

Source Evaluation: Also published in the reputable, peer-reviewed journal Scientific Reports. The authors have backgrounds in medical imaging, computational neuroscience, and software development, showing credibility in this subject field. Having currently been cited well in excess of 100 times, it shows the impact this paper has had and the relevance it has throughout the scientific community.

1.4.3 Lesion Network Mapping for Symptom Localization

Citation: Joutsa et al. (2022)

Overview: A review of lesion network mapping, including methodology and applications of lesion network mapping.

Relevance: Shows the development and uses of lesion network mapping, including multiple techniques. This has a very useful table with the papers in which disorders and symptoms have been localised using lesion network mapping. We can use this to find information about the different lesion networks formed within this research.

Source Evaluation: Published in Current Opinion in Neurology, a reputable, peer-reviewed journal with high standards, the authors have credible backgrounds in their respective fields of study, and this paper has been cited multiple times.

1.4.4 The Role of the Corpus Callosum in Seizure Spread

Citation: Wiesmann et al. (2015)

Overview: An investigation into the relationship between tumour localisation and seizure generalisation using quantitative lesion mapping on magnetic resonance images.

Relevance: This paper's focus is similar to this project's as it lesion maps Oligodendrogloma tumours, whereas we will be lesion mapping meningiomas. This paper will be a great reference for how a tumour interacts with other regions of the brain through lesion networking. However, our study is a methods evaluation and we don't make any clinical interpretations such as this paper does.

Source Evaluation: published in Epilepsy Research, a reputable, peer-reviewed journal, this paper, written by academics such as Uwe C. Wiesmann and others, who have credible backgrounds in neurology, neuroimaging, and epilepsy research, has been cited multiple times.

2 Methodology

2.1 Material and Participants

The pipeline was run on Ubuntu 22.04 jammy jellyfish, requiring a minimum of 24 GB of system RAM to complete some of the more resource-intensive processes within the pipeline, which was constructed using several neuroscientific software libraries, including but not limited to ANTs, MRtrix3, FreeSurfer, FSL. (Fischl, 2012; Jenkinson et al., 2012; Tournier et al., 2019; Tustison et al., 2021). Code used in this project is available in the appendix (Section 5).

We are using data that was provided by the Liverpool Neuroscience Biobank and initially collected by the NHS Walton Centre Foundation Trust, we have 5 subjects diagnosed with meningioma. For our healthy control patients used to generate the normative white matter template, we have 45 subject scans from the EPINET project, an epilepsy research study carried out by the University of Liverpool, under the supervision of Professor Simon Keller. All subject data is pre-anonymised before we gain access. the subject scans are all clinical heterogeneous scans, whereas the normative DWI scans are all homogeneous diffusion kurtosis scans with bvals of 1000 and 2500 and 64 bvecs at each shell.

2.2 Meningioma Image Preprocessing

Within this stage, we take the meningioma patient structural MRI scans and begin with pre-processing the image. We first applied bias field correction using

the ANTs N4BiasFieldCorrection tool, which corrected low-frequency intensity non-uniformity, omitting any erroneous intensity variation throughout the data. Then we resampled the image to an isotropic resolution using the MRtrix3 tool mrgrid, which standardises the image resolution across the dataset, where variation could occur from the use of different sequences. This step also makes the image input to the automated meningioma segmentation algorithm the most similar to the training data, which ensures the best performance. Next, the image is skull stripped using the FreeSurfer tool mri_synthstrip, should this fail, we would use the fsl tool bet as an alternative, accomplishing the same objective, skull stripping segments the brain tissue from the skull and dura, improving reliability.

2.3 The Normative Data Pipeline

Within this stage, we initially take the bvec and bval files, containing metadata used when estimating the direction of fibres in the direction image. A reverse b0 image is created, which is gradient free and contains the information needed to correct for susceptibility distortions, because it is acquired "back to front" in comparison to the main image; when combined, the distortions present in each image cancel each other out. Then, using dwidenoise from MRtrix3, we removed any random noise present before using mrdegibbs also from MRtrix3, which removed Gibbs ringing artefacts. We then created the b0 pair image for use in topup and eddy correction. The MRtrix3 wrapper for FSL's topup and eddy process was applied, removing any bias created by collecting signal in one direction and removing eddy currents. The DWI series was then upsampled to 1.25mm isotropic resolution. The DWI series was then averaged, which creates a singular image for mri_synthstrip, which estimates a mask of the brain, extracting it from the cranium. The individual patients tissue responses are then estimated from the full series.

All of the tissue responses over the set of healthy control patients are then averaged. The individual DWI images undergo spherical deconvolution to estimate the fibre orientation distributions (FODs) from the diffusion signal, using the computed average response functions. Global signal normalisation is carried out in each FOD image. The normalised white matter fibre orientation distribution images (WMFOD) are non-linearly warped together, which creates a population-specific template image of the white matter and FODs. Individual WMFOD images are non-linearly registered to template space, providing subject DWI-to-template warps. Individual DWI masks are warped to template space using those template warps. The minimum overlap of the subject masks is computed and used to bound any fixel-wise and fibre tracking operations to a common subject space. The template mask and the population WMFOD template are used to estimate template fixels. Using the WMFOD template, we generate a tractogram with 40 million tracts seeded across the WMFOD template brain, which is then sifted down to 1 million tracts, increasing the anatomical validity of the tracts remaining. A fixel connectivity matrix is then generated for analysis beyond the initial scope of this study.

2.4 The Subject Specific Pipeline

The now bias field corrected, resampled, and skull stripped structural image produced from the Meningioma image preprocessing stage is then registered to the WMFOD template image using the FSL tool, flirt. This is to standardise the spatial alignment within the dataset across different patients. The next step was to delineate each patient’s meningioma manually (from the upscaled isotropic image before skull stripping). For this, we drew ROIs in MRView, which were then visually checked by CR for accuracy. For the automatic delineation of the meningiomas, we used the Nobrainer Docker container as recommended on the neuronets GitHub repository, as it contains all the dependencies required to use the framework. This step returns a mask of the meningioma (derived also from the resampled image before skull stripping). The resultant mask can, however, include erroneous segmentations. To remove these segmentations, we order them by size using the AFNI 3dClusterise tool, then remove with fsmaths from FSL, leaving only the largest delineation. Both manual and automatic masks are then warped into subject space.

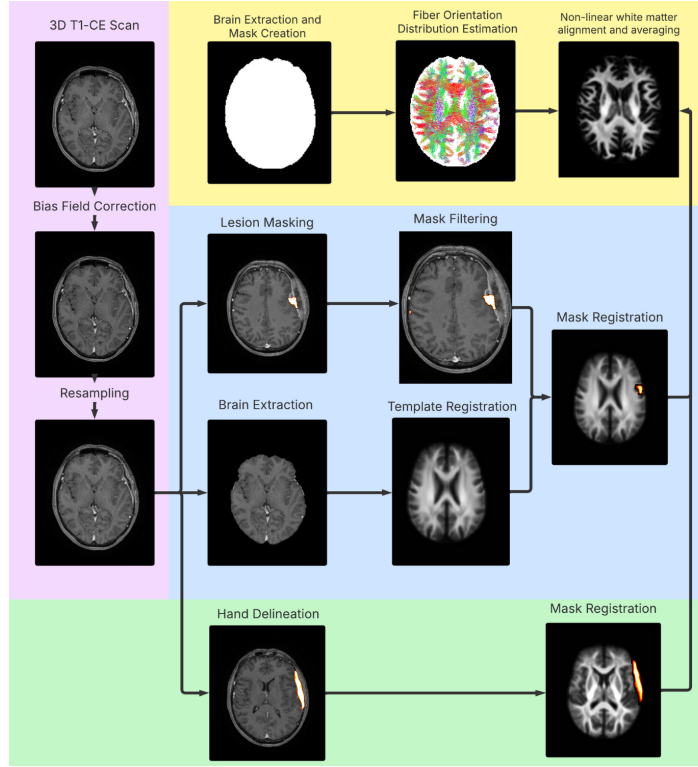


Figure 1: Each background colour indicates the part of the pipeline within it. Pink: Meningioma Image Preprocessing, Yellow: The Normative Data Pipeline, Blue: Subject Specific Pipeline, Green: Hand delineation

2.5 Statistical Analysis

We have chosen appropriate statistical analysis methods to quantify the differences between manually and automatically produced masks. The following tests directly compare the accuracy of the pipeline in both producing a delineation as well as the downstream effects of using the mask for seeded tractograms. A method we chose was to take the difference in voxel count between the manual and automatic masks, then the square root of the sum of the two masks and divide the difference by that square root. This shows the magnitude of voxel count differences, using this value and the conversion system defined in The simplest statistical test: how to check for a difference between treatments (Pocock, 2006) to take the value of Z and get a p value.

$$Z = \frac{|V_1 - V_2|}{\sqrt{V_1 + V_2}}$$

we used a paired t-test because we are comparing the same subject in two different conditions. A p-value of less than .050 indicates that the datasets are statistically significantly different. another method to measure the difference between the datasets is by using the Sørensen–Dice index.

$$DSC = 2 \times \frac{|A \cap B|}{|A| + |B|}$$

We sum together the binarised volumes of the manual and automatic seeded lesion tractograms. We then multiply the 2 binarised images, which leaves only the overlapping volume between the 2 masks or common voxels. We then multiply the overlap by 2. Having been used to validate several image segmentation and tissue segmentation algorithms (Yao et al., 2020), the Sørensen–Dice index is very broadly used and provides great insight into the similarity between two sets of data, in our case, the manual mask and the automatic mask.

Using mrstats from MRtrix3 and its in-built option -ignorezero, we can count the number of voxels each tractogram passes through, quantifying the size difference between the tractograms. This will, in turn, show the scale of the downstream differences when tractograms are seeded from the masks. We can also compare the size of the lesion mask in voxels / 1.25 mm³. These two comparisons are simple yet will show a lot of differences between the masks and allow easy quantitative analysis during discussion.

We also used a subtraction map to compare tractograms since the dice overlap compares binary voxel overlap rather than the overlapping of streamlines that pass through. Some voxels will contain only single tracts, but others will contain hundreds. This information is lost when binarising for DSC. The tracking algorithm used the same parameters each time, which means the tractograms should be comparable.

3 Results

Subject	Manual V_1	Automatic V_2	Magnitude Z	p Score
001	255333	209329	67.49	<.001
002	375002	377931	3.38	<.001
003	318814	323569	5.93	<.001
004	276779	234129	59.67	<.001
005	259556	266938	10.17	<.001

Table 1: magnitude of tractography differences calculated per subject. Manual and Automatic columns are shown in voxel count or voxels traversed.

The magnitude of difference between the automatically generated masks and ranges between 67.49 and 3.38, when converted using the mechanism defined in (Pocock, 2006), we get unanimous p scores of <0.001. The size of the manual tractographs in voxels traversed ranges between 255333 and 375002, whereas the automatic masks have a much larger range between 209329 and 377931.

Subject	Manual Mask Size mm ³	Automatic Mask Size mm ³	Magnitude Z	P Score
001	63929	16716	166.25	<.001
002	88371	76830	28.39	<.001
003	53025	59382	18.96	<.001
004	30171	7267	118.37	<.001
005	15080	17279	12.22	<.001

Table 2: Statistics derived from manual and automatically delineated masks

The magnitude of difference between the automatically generated masks and ranges between 166.25 and 12.22, when converted using the mechanism defined in (Pocock, 2006), we get unanimous p scores of <0.001. The size of the manual mask in mm³ ranges between 15080 and 88371, whereas the automatic masks have a similar range between 7267 and 76830.

T-Test results on the mask sizes: T-statistic: 1.51, P-value: .204

The paired t-test ran on our mask sizes returns a t-stat of 1.51, which translates to a p-value of .204 for this sample size (n=5)

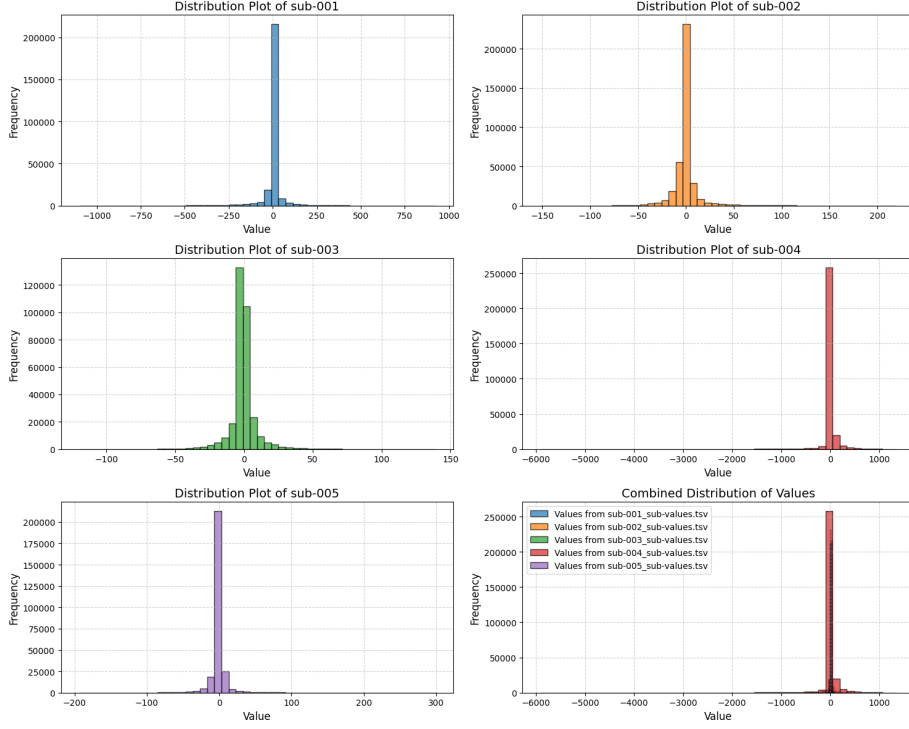


Figure 2: distribution plot of the subjects' vectors with 0s removed

These plots show the distribution of values from each masks vector, any values of 0s are removed for visibility as the majority of the mask is 0s indicating where there is not a mask.

Subject	Manual Mask Voxels	Automatic Mask Voxels	Overlapping Mask Voxels	DSC
001	32732	8559	7220	0.34
002	45246	39337	37660	0.89
003	27149	30404	26717	0.92
004	15448	3721	2068	0.21
005	7721	8847	7597	0.91

Table 3: Statistics derived from calculating the Sørensen–Dice index

The overlapping voxels of manual and automatically delineated voxels range from 2068 up to 37660, and the DCS range is from 0.21 to 0.92.

Subject	median	Standard Deviation	Min	Max
001	1	70.68	-1101	923
002	-1	14.53	-152	220
003	-1	9.97	-120	139
004	1	208.96	-5910	1353
005	-1	12.78	-194	299

Table 4: Statistics derived from the subtraction image of the tractograms

Median of each subject's subtraction image is either -1 or 1, and the standard deviation ranges between 9.97 and 208.96. Min or minimum intensity value ranges from -5910 to -120, whereas the maximum is from 139 to 1353.

3.1 Mask Comparison

This section shows specific axial slices of subjects 001 through 005 that show how the pipeline preformed in context of the manual delineation, the slices shown for each subject, are intended to show the most visually identifiable flaws of the mask or in cases where the delineations are almost indistinguishable a slice which has the most variance is shown.

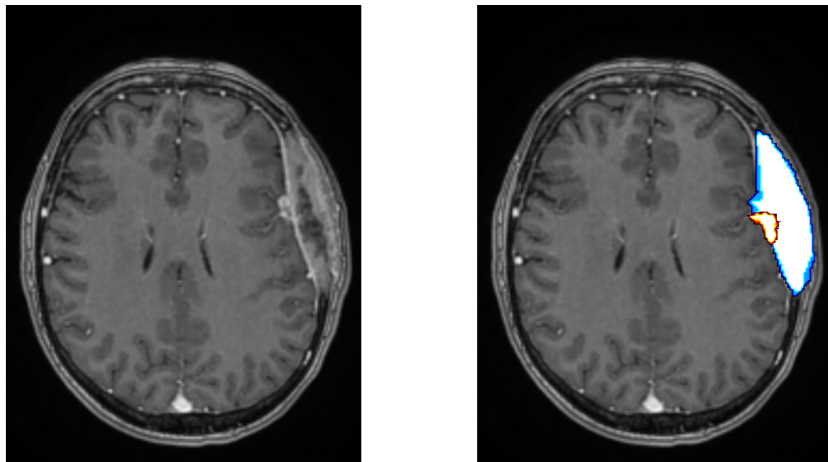


Figure 3: Left: an axial slice Sub-001, Right: The same axial slice with the automatic (Red/Orange outline) and manual mask (Blue outline) overlayed

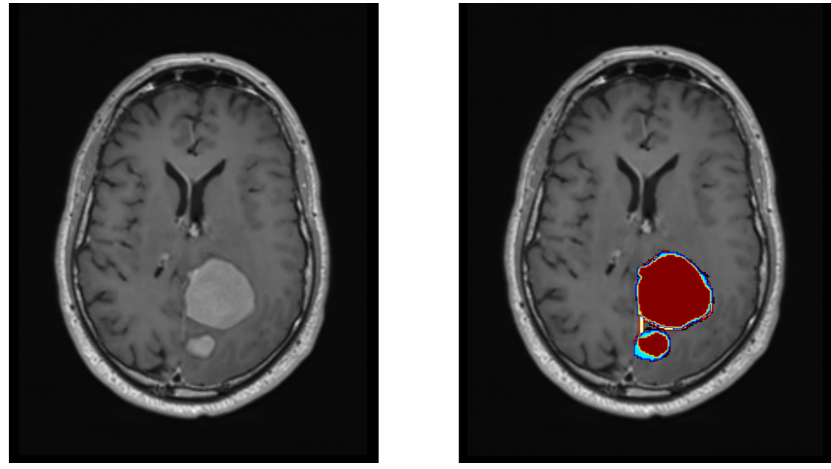


Figure 4: Left: an axial slice Sub-002, Right: The same axial slice with the automatic (Red/Orange outline) and manual mask (Blue outline) overlayed, they are almost identical and hard to differentiate

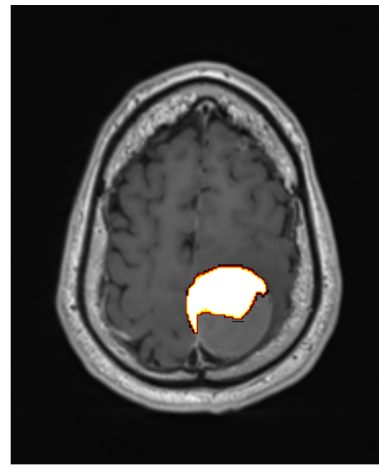


Figure 5: an axial slice of Sub-002, where some of the tumour has been incorrectly segmented

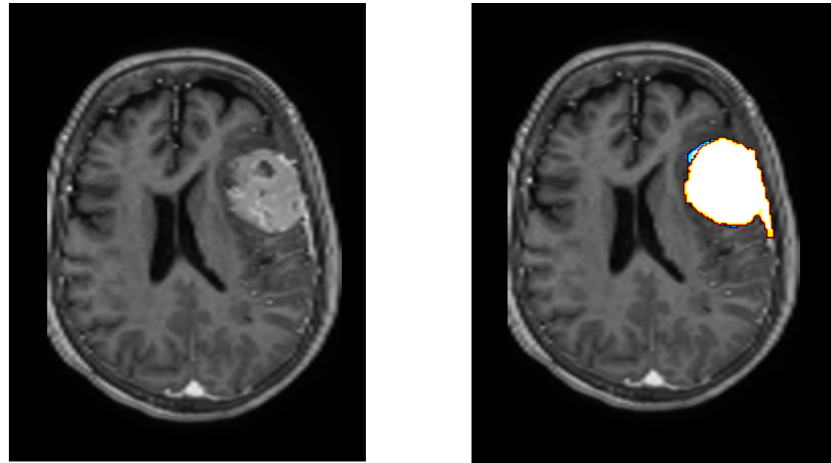


Figure 6: Left: an axial slice Sub-003, Right: The same axial slice with the automatic (Red/Orange outline) and manual mask (Blue outline) overlayed, they are almost identical and hard to differentiate

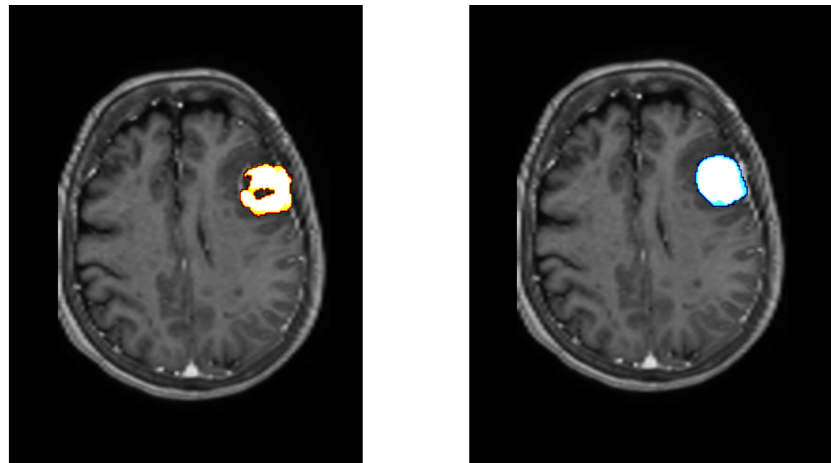


Figure 7: Left: an axial slice Sub-003 automatically delineated, leaving a central gap in the middle of the mask, Right: the same slice with the manual delineation overlayed

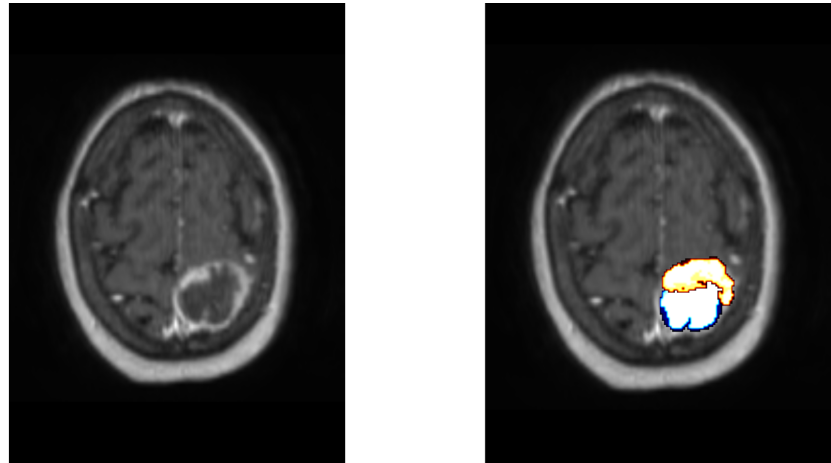


Figure 8: Left: an axial slice Sub-004, Right: The same axial slice with the automatic (Red/Orange outline) and manual mask (Blue outline) overlayed

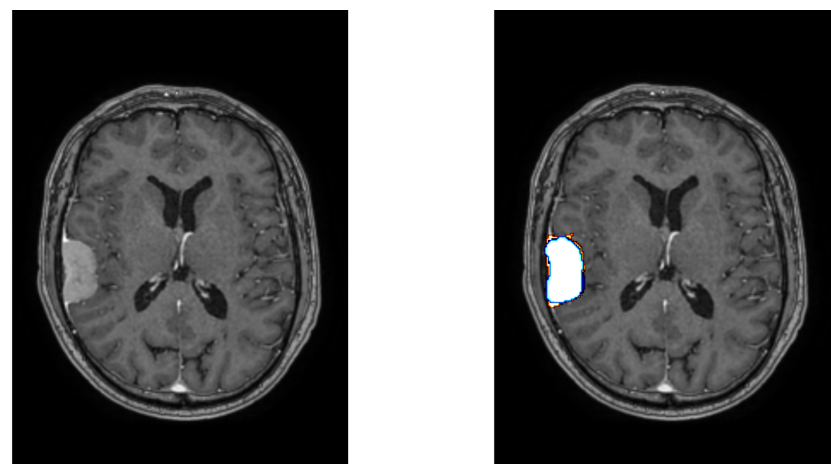


Figure 9: Left: an axial slice Sub-005, Right: The same axial slice with the automatic (Red/Orange outline) and manual mask (Blue outline) overlayed

4 Discussion

The objective of this study was to evaluate the feasibility of automated lesion masking for normative lesion network mapping, and in that context, we can interpret these results. Upon looking at the results, it's obvious from the p-values that the manual and the automatic masks produce statistically dissimilar results. This, at face value, shows strong evidence to suggest that the pipeline is not a feasible alternative to manual delineation, nor do the resulting seeded tractograms bear much resemblance. However, for use in a research capacity where approximations across large datasets are required, it shows promise.

4.1 Mask Comparison

In some cases, the larger variance between some masks can be explained, such as that of subject 001. As shown in Figure 3, while masking the lesion present in subject 001's scans, the pipeline tends not to include extremities that don't infiltrate the brain; there is an argument that the completeness of the manually delineated mask is unnecessary, since the majority of the manual mask encompasses a Peritumoural oedema that was present, which has been shown to be associated with seizure activity (Baris et al., 2016). The majority of the mask of the first subject is outside the brain, hence most of the tumour in the same space has been captured in the automatic mask. Figure 2 shows the size difference caused by this, with the manual mask being over 3 times the size of the automatic mask and a P score of $<.001$ showing a major statistical difference between the two masks.

As for subject 002, Figure 4 shows an axial slice where an almost identical delineation has been produced by hand and by automatic delineation, and throughout the majority of the image, the delineations are nearly indistinguishable from one another, as reflected by the DSC shown in Table 3 being 89%, however where the pipeline has underperformed is in the upper extremity of the tumour as shown in Figure 5, this slice is positioned 15 slices below the most superior slice in which a manual delineation occurs and it is where the segmentation accuracy of the tumour tissue starts to deteriorate.

Subject 003 managed to achieve the highest Dice similarity coefficient recorded within the dataset at 92%, it delineated the lesion with very high accuracy as shown in Figure 6. This mask showed an interesting difference between the manual delineation and the pipeline, the tissue segmentation software didn't delineate an inner section of the meningioma. While delineating the masks manually, the outline of the meningioma was first traced, and then simply filled; the tissue left unmasked by the segmentation software is inherently tumorous, however, for use in tractography, a cavity left unmasked within the tumour would not substantially affect the resulting seeded tractogram.

In contrast, subject 004 yielded the lowest resulting DSC, with the manual mask being over 4 times the size, detailed in Table 2. And while subject 001 obtained a relatively similar low DSC score, the causes are very different; here, the pipeline struggled to delineate the majority of the meningioma with no

immediately obvious reason, whereas in subject 001's delineations, the low score is due to a difference in defining mask boundaries.

Subject 005 achieved a 91% DSC, as shown in Table 2 and proved to be very accurate at delineating the lesion. Over the whole dataset, the mean DSC was 65%. In the paper that debuted the meningioma segmentation software used in the pipeline "Deep neural networks allow expert-level brain meningioma segmentation and present potential for improvement of clinical practice" (Boaro et al., 2022), they test the same meningioma segmentation algorithm and were able to achieve a mean tumour segmentation Dice score of 85%, in our dataset used for testing we have 5 subjects with meningiomas, however their test set contained 67 subjects containing meningiomas a stark difference in amount of test subjects. Given the difference in the masks produced from subject 2's scans (shown in Figure 4) there could be an argument that if the expert delineated on the infiltrating part of the meningioma the mean DSC could more closely resemble the one presented in their debutant paper but the majority of the difference can seemingly be boiled down to the amount of subjects we have. However the measure of this pipeline's suitability for use in a research capacity, specifically tractography-based studies, doesn't depend upon mimicking gold standard delineation accuracy, but rather on achieving a high enough accuracy that the resulting tractographs seeded from a manual and an automatic delineation of the same lesion are close enough that it still produces usable data while gaining the benefit of automaticity, cost reduction and time reduction. currently, this pipeline wouldn't reap many of these benefits if implemented to process subject data on an individual basis, where it would shine is on a large scale, where a big set of subject scans requires delineation to a good standard.

4.2 Tractography Comparison

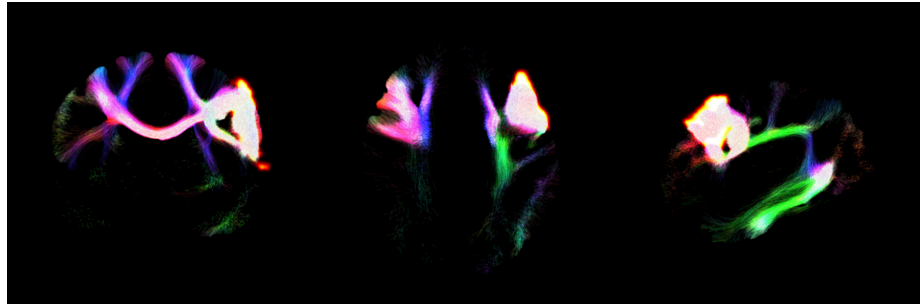


Figure 10: ortho view of the subject 001 automatic mask and seeded tractography, Left: Coronal, Middle: Axial, Right: Saggital

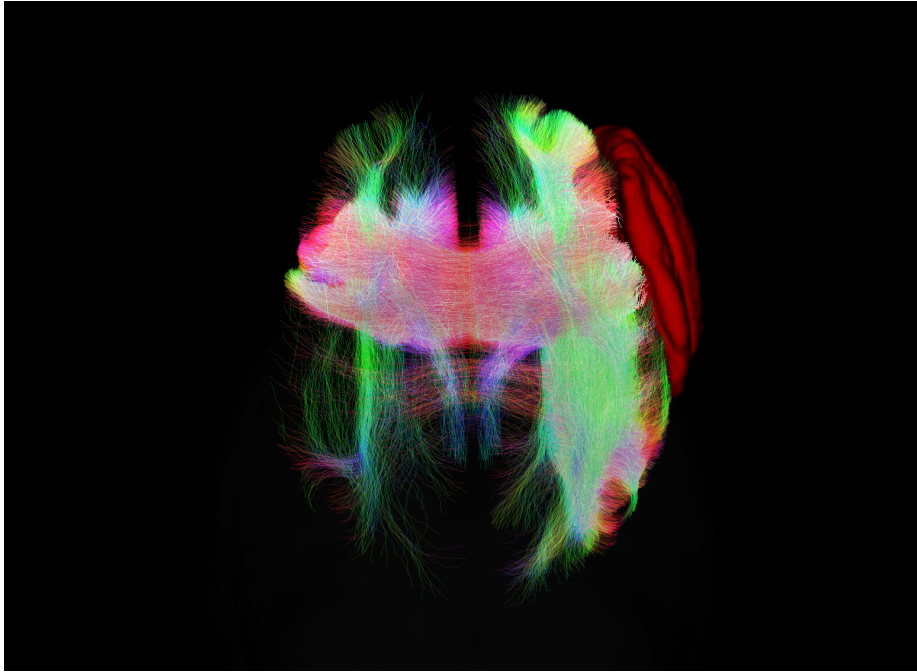


Figure 11: Subject 001 hand delineated mask with seeded tractogram volume rendered, red mass on the right is the delineation

Tractography is a novel technique that is gaining momentum; it has many uses in patients diagnosed with brain tumours such as before resection tractography is commonly used to map out tracts for functional networks (i.e. distributed areas used to produce behaviour, like speech) and factoring in how close they are to the resection needs to be resected this can help when planning surgical resection and predicting risks for the patient who is set to undergo the surgery. Figures 10 and 11 show examples of this. This assists in tumour resection while avoiding new postsurgical deficits (Yeh et al., 2021). The tumour segmentation Dice score has a very high correlation with the difference in voxels traversed. This implies that the closer the masks resemble each other / the higher the DSC, the lower the difference between the tractograms. In subjects 001 and 004, the DSC was substantially lower than in subjects 002, 003 and 005. When the dice score is high, the seeded tractograms show very little difference in voxels traversed, as shown in Table 1.

The magnitude of difference or Z in Tables 1 and 2 shows the size of the difference between the manual and automatic masks, and across all 5 subjects, the magnitude of voxels traversed during tractography is lower than the magnitude of difference in delineated mask voxel counts, much lower in fact and with the p score also significant (at <0.050), the discrepancies between manual and automatic methods are consistent and not due to random variation. in subjects 002, 003 and 005 there is not enough difference in the tractograms to

impact the prediction of the focal effect of the tumour to distal regions of the brain and as stated previously, there are reasons the mask of subject 001 is significantly different, leading it to possibly be skewing the results due to a difference in masking boundaries defined by the manual and automatic delineation rather than a bad mask. which, assuming that had sub 001 been delineated in a more congruent style (the manual delineation not including the Peritumoural oedema in the mask) the tractograms would have been closer in size. Only 1/5 of the tractographs produced from automatic delineation would have been affected enough by the automatic masking of their lesion to become erroneous.

4.3 Limitations & Future Plans

Comparison of the time taken to complete the 5 subjects when done manually against manual delineation. This would've been an interesting test to conduct, as one of the major benefits of using automatic lesion masking is time reduction. Still, for this test to be useful, the pipeline would have to run on up-to-date, publicly available hardware. Unfortunately, the majority of this pipeline was run on a relatively out-of-date system, with the majority of the hardware considered modern back in 2019.

Our set of meningioma patients was limited; if we were able to procure more scans of patients diagnosed with meningioma, we could use them to evaluate the performance of the pipeline on more types of meningioma, in different regions of the brain with different lesion maps produced from them, in turn giving us more data to provide a better, more accurate analysis of the pipelines overall preformance.

The fibre tracking could be improved by exploration of different parameters and in different combinations, which would allow comparison between parameters.

Another potential area for exploration is using functional connectivity, blood flow, similar to a seeded tractograph, which offers a quantitative and reliable measurement for brain activity and is increasingly used to study functional networks (Wu et al., 2025). Using it as another method to predict functional networks could add another dimension to the testing of automatic lesion delineation.

4.4 Conclusion

Lesion masking is a time-consuming and expensive but it is currently the gold standard for the delineation of meningiomas. This paper's goal was to evaluate whether the implementation of a pipeline that automatically delineates lesions is feasible for use in normative lesion network mapping. Though clinical use of the pipeline is not currently advisable due to the variance between the masks produced, use of this pipeline in a research capacity shows a lot of promise, with the seeded tractograms having a high enough accuracy to not deviate the reported connectivity too far from the tractogram seeded from the manually delineated mask causing inaccuracies in predictions of focal effects. It's quicker

than manual delineation and is autonomous, meaning less expert time is required to complete the delineations needed to produce research. This is invaluable for large datasets, which could take weeks or months to delineate, requiring an experienced professional to dedicate a substantial amount of time towards delineation.

In effect, the use of automated lesion masking for normative lesion network mapping offers many benefits with a small trade-off for accuracy, which in a large-scale research capacity could be the difference between a research project being viable or unviable.

References

- Bammer, R., Acar, B., & Moseley, M. E. (2003). In vivo MR tractography using diffusion imaging. *European Journal of Radiology*, 45(3), 223–234. [https://doi.org/10.1016/S0720-048X\(02\)00311-X](https://doi.org/10.1016/S0720-048X(02)00311-X)
- Baris, M. M., Celik, A. O., Gezer, N. S., & Ada, E. (2016). Role of mass effect, tumor volume and peritumoral edema volume in the differential diagnosis of primary brain tumor and metastasis. *Clinical Neurology and Neurosurgery*, 148, 67–71. <https://doi.org/10.1016/j.clineuro.2016.07.008>
- Basser, P. J., Mattiello, J., & LeBihan, D. (1994). MR diffusion tensor spectroscopy and imaging. *Biophysical Journal*, 66(1), 259–267. [https://doi.org/10.1016/S0006-3495\(94\)80775-1](https://doi.org/10.1016/S0006-3495(94)80775-1)
- Behling, F., Hempel, J.-M., & Schittenhelm, J. (2021). Brain Invasion in Meningioma—A Prognostic Potential Worth Exploring. *Cancers*, 13(13), 3259. <https://doi.org/10.3390/cancers13133259>
- Boaro, A., Kaczmarzyk, J. R., Kavouridis, V. K., Harary, M., Mammi, M., Dawood, H., Shea, A., Cho, E. Y., Juvekar, P., Noh, T., Rana, A., Ghosh, S., & Arnaout, O. (2022). Deep neural networks allow expert-level brain meningioma segmentation and present potential for improvement of clinical practice. *Scientific Reports*, 12(1), 15462. <https://doi.org/10.1038/s41598-022-19356-5>
- Boes, A. D., Prasad, S., Liu, H., Liu, Q., Pascual-Leone, A., Caviness, V. S., & Fox, M. D. (2015). Network localization of neurological symptoms from focal brain lesions. *Brain*, 138(10), 3061–3075. <https://doi.org/10.1093/brain/awv228>
- Englot, D. J., Magill, S. T., Han, S. J., Chang, E. F., Berger, M. S., & McDermott, M. W. (2016). Seizures in supratentorial meningioma: A systematic review and meta-analysis. *Journal of Neurosurgery*, 124(6), 1552–1561. <https://doi.org/10.3171/2015.4.JNS142742>
- Fischl, B. (2012). FreeSurfer. *NeuroImage*, 62(2), 774–781. <https://doi.org/10.1016/j.neuroimage.2012.01.021>
- Fisher, R. S., Cross, J. H., French, J. A., Higurashi, N., Hirsch, E., Jansen, F. E., Lagae, L., Moshé, S. L., Peltola, J., Roulet Perez, E., Scheffer, I. E., & Zuberi, S. M. (2017). Operational classification of seizure types by the International League Against Epilepsy: Position Paper of the ILAE Commission for Classification and Terminology. *Epilepsia*, 58(4), 522–530. <https://doi.org/10.1111/epi.13670>
- Gupte, T. P., Li, C., Jin, L., Yalcin, K., Youngblood, M. W., Miyagishima, D. F., Mishra-Gorur, K., Zhao, A. Y., Antonios, J., Huttner, A., McGuone, D., Blondin, N. A., Contessa, J. N., Zhang, Y., Fulbright, R. K., Gunel, M., Erson-Omay, Z., & Moliterno, J. (2020). Clinical and genomic factors associated with seizures in meningiomas. *Journal of Neurosurgery*, 135(3), 835–844. <https://doi.org/10.3171/2020.7.JNS201042>
- Hu, R., & Hoch, M. J. (2021). Application of Diffusion Weighted Imaging and Diffusion Tensor Imaging in the Pretreatment and Post-treatment of

- Brain Tumor. *Radiologic Clinics of North America*, 59(3), 335–347. <https://doi.org/10.1016/j.rcl.2021.01.003>
- Jenkinson, M., Beckmann, C. F., Behrens, T. E. J., Woolrich, M. W., & Smith, S. M. (2012). FSL. *NeuroImage*, 62(2), 782–790. <https://doi.org/10.1016/j.neuroimage.2011.09.015>
- Joutsa, J., Corp, D. T., & Fox, M. D. (2022). Lesion network mapping for symptom localization: Recent developments and future directions. *Current opinion in neurology*, 35(4), 453–459. <https://doi.org/10.1097/WCO.0000000000001085>
- Moody, J. F., Adluru, N., Alexander, A. L., & Field, A. S. (2021). The Connectomes: Methods of White Matter Tractography and Contributions of Resting State fMRI. *Seminars in Ultrasound, CT and MRI*, 42(5), 507–522. <https://doi.org/10.1053/j.sult.2021.07.007>
- O'Connor, P. J. (1990). Normative data: Their definition, interpretation, and importance for primary care physicians. *Family Medicine*, 22(4), 307–311.
- Ostrom, Q. T., Cioffi, G., Waite, K., Kruchko, C., & Barnholtz-Sloan, J. S. (2021). CBTRUS Statistical Report: Primary Brain and Other Central Nervous System Tumors Diagnosed in the United States in 2014–2018. *Neuro-Oncology*, 23(Supplement_3), iii1–iii105. <https://doi.org/10.1093/neuonc/noab200>
- Pocock, S. J. (2006). The simplest statistical test: How to check for a difference between treatments. *BMJ : British Medical Journal*, 332(7552), 1256–1258.
- Rajchl, M., Pawlowski, N., Rueckert, D., Matthews, P. M., & Glocker, B. (2018, June). NeuroNet: Fast and Robust Reproduction of Multiple Brain Image Segmentation Pipelines. <https://doi.org/10.48550/arXiv.1806.04224>
- Tournier, J.-D., Smith, R., Raffelt, D., Tabbara, R., Dhollander, T., Pietsch, M., Christiaens, D., Jeurissen, B., Yeh, C.-H., & Connelly, A. (2019). MRtrix3: A fast, flexible and open software framework for medical image processing and visualisation. *NeuroImage*, 202, 116137. <https://doi.org/10.1016/j.neuroimage.2019.116137>
- Tustison, N. J., Cook, P. A., Holbrook, A. J., Johnson, H. J., Muschelli, J., Devenyi, G. A., Duda, J. T., Das, S. R., Cullen, N. C., Gillen, D. L., Yassa, M. A., Stone, J. R., Gee, J. C., & Avants, B. B. (2021). The ANTsX ecosystem for quantitative biological and medical imaging. *Scientific Reports*, 11(1), 9068. <https://doi.org/10.1038/s41598-021-87564-6>
- Wieshmann, U. C., Milinis, K., Paniker, J., Das, K., Jenkinson, M. D., Brodbelt, A., Crooks, D., & Keller, S. S. (2015). The role of the corpus callosum in seizure spread: MRI lesion mapping in oligodendrogiomas. *Epilepsy Research*, 109, 126–133. <https://doi.org/10.1016/j.eplepsyres.2014.10.023>
- Wu, C., He, Y., Li, J., Qiu, X., Zou, Q., & Wang, J. (2025). A novel method for functional brain networks based on static cerebral blood flow. *NeuroImage*, 308, 121069. <https://doi.org/10.1016/j.neuroimage.2025.121069>

- Yao, A. D., Cheng, D. L., Pan, I., & Kitamura, F. (2020). Deep Learning in Neuroradiology: A Systematic Review of Current Algorithms and Approaches for the New Wave of Imaging Technology. *Radiology: Artificial Intelligence*. <https://doi.org/10.1148/ryai.2020190026>
- Yeh, F.-C., Irimia, A., Bastos, D. C. d. A., & Golby, A. J. (2021). Tractography methods and findings in brain tumors and traumatic brain injury. *NeuroImage*, 245, 118651. <https://doi.org/10.1016/j.neuroimage.2021.118651>

5 Appendix

5.1 Structural Pipeline Code

```
idu=1000 # run id -u in terminal
idg=1000 # run id -g in terminal

cd ../derivatives/templates
mrconvert \
    template-space_mask.mif \
    bet-avg.nii.gz

cd ../../meningioma_raw_data
# make a folder for the results of each pipeline run on T1-CE Scans

for i in sub-*_T1.nii.gz # loop through each image
do
    cd ../derivatives/meningioma_patients # enter the structural
    derivatives folder
    mkdir ${i:0:7} # create files for each of the T1 image
    derivatives
done

cd ../../meningioma_raw_data
echo "Starting Loop"
for i in sub-*_T1.nii.gz # for testing purposes, the T1 images are in
one directory
do
    identifier=${i:0:7}
    brain=${identifier}_T1.nii.gz
    echo $brain
    # Checking if bias field correction has already been
    completed
    if [[ ! -e ../derivatives/meningioma_patients/${{
        identifier}}/${{identifier}}_biascorr.nii.gz ]]
    then
        #Bias Field Correction
        N4BiasFieldCorrection \
            -i $brain \
            -o ../derivatives/
            meningioma_patients/
            ${{identifier}}/${{identifier}}
            _biascorr.nii.gz
        echo "Bias Field Corrected on Brain ID: ${{
            identifier}}"
    else
        echo "Already done bias field correction"
    fi
    cd ../derivatives/meningioma_patients/${{identifier}}
    # Checking if Resampling has already been completed
    if [[ ! -e ${{identifier}}_iso.nii.gz ]]
    then
        #Resample
        mrgrid \
            ${{identifier}}_biascorr.
            nii.gz \
            regrid \
            -voxel 1.00 \
            ${{identifier}}_iso.nii.
            gz
        echo "Resampled Brain ID: ${{identifier}}"
    else
        echo "Already Resampled"
    fi
done
```

```

# Checking if Skull Strip has already been completed
if [[ ! -e ${identifier}_bet.nii.gz ]]
then
    #Skull Strip
    mri_synthstrip \
        -i ${identifier}_iso.\
            nii.gz \
        -o ${identifier}_bet.\
            nii.gz
    if [[ ! -e ${sub}_bet.nii.gz ]]
    then
        echo "Using FSL instead"
        bet \
            ${identifier}_iso.nii.gz \
            ${identifier}_bet.nii.\
                gz -B
    fi
    echo "Skull Stripped Brain ID: ${identifier}"
else
    echo "Already Skull Stripped"
fi

# Checking if stripped template registration has already
# been completed
if [[ ! -e ${identifier}_bet2std.nii.gz ]]
then
    #registered to the stripped template image
    flirt \
        -omat ${identifier}\
            _bet2std.mat \
        -in ${identifier}_bet.\
            nii.gz \
        -ref ../../derivatives/\
            templates/bet-avg.\
            nii.gz \
        -out ${identifier}\
            _bet2std.nii.gz
    echo "registered to the stripped template image ,\
        Brain ID: ${identifier}"
else
    echo "Already registered to the stripped\
        template image"
fi

# Checking if masking has already been completed
if [[ ! -e ${identifier}_mask.nii.gz ]]
then
    sudo docker run -it --rm -v $(pwd):/data --user
        ${idu}:${idg} neuronets/ams:latest -cpu ${\
            identifier}_iso.nii.gz ${identifier}_mask
    echo "Meningioma Masked , Brain ID: ${identifier}"
else
    echo "Already masked meningioma"
fi

# check if the refinement is done
if [[ ! -e ${identifier}_roi.nii.gz ]]
then
    echo "clusterising"
    #clusterising map
    3dClusterize \
        -inset ${identifier}_mask_orig.\
            nii.gz \
        -ithr 0 \
        -idat 0 \
        -clust_nvox 1 \

```

```

        -NN 3 \
        -bisided 0 1 \
        -pref_map ${identifier}_map.nii
        .gz
echo "Meningioma Clusterised , Brain ID: ${
        identifier}
fslmaths \
        ${identifier}_map.nii.gz \
        -uthr 1 \
        ${identifier}_roi.nii.gz

echo "leaving only the largest cluster , Brain
ID: ${identifier}
else
    echo "Already refined mask"
fi

# Checking if registration to white space template has
# already been completed
if [[ ! -e ${identifier}_space-temp_roi.nii.gz ]]
then
    flirt \
        -in ${identifier}_roi.
        nii.gz \
        -ref ../../..
        derivatives/
        templates/bet-avg.
        nii.gz \
        -init ${identifier}
        _bet2std.mat \
        -applyxfm \
        -out ${identifier}
        _space-temp_roi.nii
        .gz
echo "Registered to template space , Brain ID: ${
        identifier}
else
    echo "Already registered to template
space"
fi
# the template-space lesion mask is converted into mif
# format, for use with tckgen
mrconvert \
        ${identifier}_space-temp_roi.nii.gz \
        ${identifier}_space-temp_roi.mif
# 100000 tracks are seeded from the template-space
# lesion, using default parameters
tckgen \
        -angle 22.5 \
        -maxlen 250 \
        -minlen 10 \
        -power 1.0 \
        ../../.. derivatives/templates/wmfod-template.
        mif \
        -seed_image ${identifier}_space-temp_roi.mif \
        -mask ../../.. derivatives/templates/template-
        space_mask.mif \
        -select 10000 \
        -cutoff 0.06 \
        ${identifier}_tractogram.tck \
        -nthreads 12
# the lesion tractograms are converted into fixel maps,
# which can be overlaid and compared
tck2fixel \
        ${identifier}_tractogram.tck \
        ../../.. derivatives/templates/fixel_mask \
        ../../.. derivatives/templates/tracks/lesion-
        tracks/ \

```

```

${identifier}_lesion-track.mif
# lesion-track pixel maps are binarised for spatial
# comparison
mrthreshold \
    ./../derivatives/templates/tracks/lesion-
        tracks/${identifier}_lesion-track.mif \
    -abs 1 \
    ./../derivatives/templates/tracks/lesion-
        tracks/${identifier}_lesion-bin.mif

cd ../../meningioma_raw_data
done

```

5.2 Diffusion Pipeline Code

```

cd ../Derivatives
mkdir Group # create group folder
cd ../_Raw_Data
for i in sub-* # loop through each file
do
    cd ../Derivatives # enter the diffusion derivatives folder
    mkdir ${i:0:7} # create files for each of the T1 image
    derivatives
    cd ${i:0:7} # create files for each of the T1 image derivatives
    mkdir anat
    mkdir dwi
    cd ../
done

cd ../_Raw_Data
echo "Starting Pipeline"
for i in sub-*
do
    sub=${i:0:7}
    DWI_Derivative_Path=../Derivatives/${sub}/dwi/
    DWI_Raw_Path=${sub}/dwi/
    mrconvert \
        -fsgrad \
            ${DWI_Raw_Path}${sub}_dir-AP_dwi.bvec \
            ${DWI_Raw_Path}${sub}_dir-AP_dwi.bval \
            ${DWI_Raw_Path}${sub}_dir-AP_dwi.nii.gz \
            ${DWI_Derivative_Path}${sub}_dwi.mif
    # extract b0 from dki series to make up PA part of phase
    # pair
    mrconvert \
        ${DWI_Derivative_Path}${sub}_dwi.mif \
        -coord \
        3 \
        0 \
        -axes 0,1,2 \
        ${DWI_Derivative_Path}${sub}_dir-AP_dwi.mif
    # convert reverse phase encoded image
    mrconvert \
        ${DWI_Raw_Path}${sub}_dir-PA_dwi.nii.gz \
        ${DWI_Derivative_Path}${sub}_dir-PA_dwi.mif
    # concatenate the phase encoding images to create the
    # phase pair
    mrcat \
        ${DWI_Derivative_Path}${sub}_dir-AP_dwi.mif \
        ${DWI_Derivative_Path}${sub}_dir-PA_dwi.mif \
        ${DWI_Derivative_Path}${sub}_acq-pair_dwi.mif \
        -axis 3
    # denoise
    dwidenoise \
        ${DWI_Derivative_Path}${sub}_dwi.mif \
        ${DWI_Derivative_Path}${sub}_dwi_denoised.mif
    # gibbs unringing

```

```

mrdegibbs \
    ${DWI_Derivative_Path}${sub}_dwi_denoised.mif \
    ${DWI_Derivative_Path}${sub}_dwi_unringed.mif \
    -axes 0,1
# eddy and topup
dwifslppreproc \
    ${DWI_Derivative_Path}${sub}_dwi_unringed.mif \
    ${DWI_Derivative_Path}${sub}_dwi_preproc.mif \
    -rpe_pair \
    -se_epi ${DWI_Derivative_Path}${sub}_acq-
        pair_dwi.mif \
    -readout_time 0.029 \
    -pe_dir AP \
    -align_seepi \
    -eddy_options "—slm=linear —nthr=8"
# bias correction
dwibiascorrect \
    ants \
        ${DWI_Derivative_Path}${sub}_dwi_preproc
            .mif \
        ${DWI_Derivative_Path}${sub}_dwi_unbiased.mif
# upsample to 1.25mm
mrgrid \
    ${DWI_Derivative_Path}${sub}_dwi_unbiased.mif \
    regrid \
    -vox 1.25 \
    ${DWI_Derivative_Path}${sub}_dwi_upsampled.mif
# mri_synthstrip to brain extract
mrconvert \
    ${DWI_Derivative_Path}${sub}_dwi_upsampled.mif \
    ${DWI_Derivative_Path}${sub}_dwi_upsampled.nii \
        .gz
fslmaths \
    ${DWI_Derivative_Path}${sub}_dwi_upsampled.nii \
        .gz \
    -Tmean \
        ${DWI_Derivative_Path}${sub}_dwi_mean_upsampled.
            nii.gz
mri_synthstrip \
    -i ${DWI_Derivative_Path}${sub}_dwi-
        mean_upsampled.nii.gz \
    -m ${DWI_Derivative_Path}${sub}_dwi-
        mask_upsampled.nii.gz
mrconvert \
    ${DWI_Derivative_Path}${sub}_dwi-mask_upsampled.
        nii.gz \
    ${DWI_Derivative_Path}${sub}_dwi-mask_upsampled.
        mif
dwi2response \
    dhollander \
        ${DWI_Derivative_Path}${sub}_dwi_upsampled.mif \
        ${DWI_Derivative_Path}${sub}_dwi_response-wm.txt \
        ${DWI_Derivative_Path}${sub}_dwi_response-gm.txt \
        ${DWI_Derivative_Path}${sub}_dwi_response-csf.txt \
        -mask ${DWI_Derivative_Path}${sub}_dwi-
            mask_upsampled.mif
done
cd ../Derivatives
echo "Starting group averaging"
for i in sub-*
do
    sub=${i:0:7}

```

```

        cp ${sub}/dwi/${sub}_dwi_response-*.txt Group
done

responsemean \
    Group/*_dwi_response-wm.txt \
    Group/group_average_response-wm.txt
responsemean \
    Group/*_dwi_response-gm.txt \
    Group/group_average_response-gm.txt
responsemean \
    Group/*_dwi_response-csf.txt \
    Group/group_average_response-csf.txt
rm Group/*_dwi_response-*.txt

for i in sub-* \
do
    sub=${i:0:7}
    dwi2fod \
        msmt_csd \
            ${sub}/dwi/${sub}_dwi_upsampled.mif \
            Group/group_average_response-wm.txt \
            ${sub}/dwi/${sub}_wmfod.mif \
            Group/group_average_response-gm.txt \
            ${sub}/dwi/${sub}_gmfod.mif \
            Group/group_average_response-csf.txt \
            ${sub}/dwi/${sub}_csf.mif \
            -mask ${sub}/dwi/${sub}_dwi- \
                mask_upsampled.mif \
            -nthreads 10
        mtnormalise \
            ${sub}/dwi/${sub}_wmfod.mif \
            ${sub}/dwi/${sub}_wmfod-norm.mif \
            ${sub}/dwi/${sub}_gmfod.mif \
            ${sub}/dwi/${sub}_gmfod-norm.mif \
            ${sub}/dwi/${sub}_csf.mif \
            ${sub}/dwi/${sub}_csf-norm.mif \
            -mask ${sub}/dwi/${sub}_dwi- \
                mask_upsampled.mif \
            -nthreads 10
    done

for i in sub-* \
do
    sub=${i:0:7}
    cp \
        ${sub}/dwi/${sub}_wmfod-norm.mif \
        Templates/FOD_Input/${sub}_fd.mif
    cp \
        ${sub}/dwi/${sub}_dwi-mask_upsampled.mif \
        Templates/Mask_Input/${sub}_pre-mask.mif
done
# create a white matter fiber orientation template
population_template \
    Templates/FOD_Input/ \
    -mask Templates/Mask_Input/ \
    Templates/wmfod-template.mif \
    -voxel_size 1.25 \
    -nthreads 4

for i in sub-* \
do
    sub=${i:0:7}
# register all of the individual wmfod images to the population template, using their masks
    mrregister \
        ${sub}/dwi/${sub}_wmfod.mif \
        -mask1 ${sub}/dwi/${sub}_dwi-mask_upsampled.mif \
        Templates/wmfod-template.mif \

```

```

        -nl_warp \
        ${sub}/dwi/${sub}_sub2template-warp.mif \
        ${sub}/dwi/${sub}_template2sub-warp.mif \
        -nthreads 4
# take the warps generated from aligning the DWI image, and
apply it to the mask
mrtransform \
    ${sub}/dwi/${sub}_dwi-mask_upsampled.mif \
    -warp ${sub}/dwi/${sub}_sub2template-warp.mif \
    -interp nearest \
    -datatype bit \
    ${sub}/dwi/${sub}_dwi-mask_template-space.mif \
    -nthreads 4
done

# compute the minimum overlap of all of the masks
mrmath \
    sub-*/*dwi/*dwi-mask_template-space.mif \
    min \
    Templates/template-space_mask.mif \
    -datatype bit \
    -nthreads 4

templatedir=../Derivatives/Templates/
# the template mask and the population template are used to estimate
template fixels
fod2fixel \
    -mask ${templatedir}template-space_mask.mif \
    -fmrls_peak_value 0.06 \
    ${templatedir}wmfod-template.mif \
    ${templatedir}fixel_mask \
    -nthreads 4
# 40mil tracks are seeded across the whole brain, using default
parameters
tckgen \
    -angle 22.5 \
    -maxlen 250 \
    -minlen 10 \
    -power 1.0 \
    ${templatedir}wmfod-template.mif \
    -seed_dynamic ${templatedir}wmfod-template.mif \
    -mask ${templatedir}template-space_mask.mif \
    -select 40000000 \
    -cutoff 0.06 \
    ${templatedir}tracks/tracks_040-mill_wholebrain.tck \
    -nthreads 4

#trim the tractogram down to a more manageable size, whilst increasing
the anatomical validity of the remaining tracks
tcksift \
    ${templatedir}tracks/tracks_040-mill_wholebrain.tck \
    ${templatedir}wmfod-template.mif \
    ${templatedir}tracks/tracks_001-mill_wholebrain_sift.tck \
    -term_number 1000000 \
    -nthreads 12
# creates a fixel-fixel connectivity matrix
fixelconnectivity \
    ${templatedir}fixel_mask/ \
    ${templatedir}tracks/tracks_001-mill_wholebrain_sift.tck \
    ${templatedir}matrix/ \
    -nthreads 12

```

5.3 Meningioma Seeded Tractography Code

```

cd ../meningioma_raw_data
echo "Starting \u2225Loop"
for i in sub-*_T1.nii.gz
do
    identifier=${i:0:7}
    cd ../derivatives/meningioma_patients/${identifier}
    tckgen \
        -angle 22.5 \
        -maxlen 250 \
        -minlen 10 \
        -power 1.0 \
        ../../../../derivatives/templates/
        wmfod-template.mif \
        -seed_image ${identifier}
        _hand_delineated_mask.mif \
        -mask ../../../../derivatives/
        templates/template-
        space_mask.mif \
        -select 100000 \
        -cutoff 0.06 \
        ${identifier}
        _hand_delineated_tractogram
        .tck \
        -nthreads 12
    # the lesion tractograms are converted
    # into fixel maps, which can be
    # overlaid and compared
    tck2fixel \
        ${identifier}_tractogram.tck \
        ../../../../derivatives/templates/
        fixel_mask \
        ../../../../derivatives/templates/
        tracks/lesion-tracks/ \
        ${identifier}
        _hand_delineated_lesion-
        track.mif
    # lesion-track fixel maps are binarised
    # for spatial comparison
    mrthreshold \
        ../../../../derivatives/templates/
        tracks/lesion-tracks/${
        identifier}
        _hand_delineated_lesion-
        track.mif \
        -abs 1 \
        ../../../../derivatives/templates/
        tracks/lesion-tracks/${
        identifier}
        _hand_delineated_lesion-bin
        .mif
done
cd ../../..

```